microorganisms

MDPI

Article

Natural Fungal Fermentation Broth of *Scleroderma bovista* Ameliorates Ulcerative Colitis by Suppressing the NF-κB Pathway and Gut Microbial Dysbiosis

Ying Yang †, Min Zhang †, Xinnuo Li, Yunqing Cheng, Siqi Yang, Hongli He, Xianjun Feng and Jianfeng Liu *

Jilin Provincial Key Laboratory of Plant Resource Science and Green Production, Jilin Normal University, Siping 136000, China

* Correspondence: jianfengliu1976@163.com

† These authors contributed equally to this work.

Abstract

Scleroderma bovista fermentation broth (SBF) exhibits anti-inflammatory activity, but its effect on ulcerative colitis (UC) remains unclear. LC-MS/MS analysis revealed that SBF contains 43 compounds, including sclerocitrin homologs, cyclic peptides, and alkaloids. In vitro, SBF (20–40 μg/mL) promoted cell viability in LPS-stimulated RAW264.7 macrophages, suppressed nitric oxide overproduction, reduced *iNOS*, *IL-1β*, and *COX-2* expression, and upregulated *IL-10* mRNA expression. In vivo, in a dextran sulfate sodium (DSS)-induced colitis model, SBF (50–200 mg/kg) dose-dependently mitigated DSS-induced weight loss, disease activity, splenomegaly, colon shortening, crypt damage, and representative images suggested a reduction in macrophage infiltration. The highest dose (SBF200) showed efficacy comparable to that of 5-ASA. Mechanistically, SBF reduced colonic IL-1β, TNF-α, and IL-6 levels and inhibited NF-κB activation by decreasing phosphorylated IκBα and p65. Colonic IL-10, which was elevated in DSS-treated mice, was lower in SBF groups than in the 5-ASA group. Furthermore, 16S rRNA sequencing showed that SBF lowered the DSS-elevated Shannon index and shifted the PCoA profiles of colitic mice toward the control group. At the genus level, SBF treatment further enriched *Akkermansia* (already elevated in DSS mice compared with controls) and increased *Faecalibaculum*, while reducing the relative abundance of *Turicibacter*, *Clostridium*, and *Enterococcus*; *Ligilactobacillus* was only partially restored and remained below control levels. Thus, SBF prophylactically mitigates DSS-induced colitis by suppressing inflammation, inhibiting NF-κB signaling, and modulating the gut microbiota, supporting further investigation of SBF as a potential fungal-derived candidate for UC treatment.

Keywords: *Scleroderma bovista* fermentation broth (SBF); ulcerative colitis; inflammation; gut microbiota; NF-κB signaling pathway

Check for updates

Academic Editor: Frank R. Stassen

Received: 4 October 2026
Revised: 5 November 2026
Accepted: 12 November 2026
Published: 18 November 2026

Copyright: © 2026 by the authors. Licensee MDPI, Basel, Switzerland. This article is an open access article distributed under the terms and conditions of the Creative Commons Attribution (CC BY) license.

1. Introduction

Inflammatory bowel disease (IBD), comprising mainly Crohn's disease and ulcerative colitis (UC), is a group of chronic, relapsing, immune-mediated disorders of the gastrointestinal tract characterized by chronic diarrhea, abdominal pain, and weight loss [1]. Its pathogenesis is driven by the interplay of genetic susceptibility, environmental triggers, gut microbiota dysbiosis, and impaired mucosal barrier function, among which intestinal barrier dysfunction is increasingly regarded as the initiating and central event [2]. Once the barrier is compromised, dysbiosis and bacterial translocation activate both innate and adaptive

immunity, thereby sustaining chronic inflammation [1]. Current evidence indicates that IBD is fundamentally a complex barrier disorder rather than a conventional autoimmune disease. Globally, the incidence of IBD continues to rise, with the prevalence of UC reaching as high as 1 in 198 individuals [2].

Currently, treatment options for UC include 5-aminosalicylic acid, corticosteroids, thiopurines, biologics, and small-molecule drugs. Nevertheless, approximately 10–20% of patients with refractory disease still require proctocolectomy [3]. Moreover, clinical responses are often suboptimal due to slow onset of action, steroid dependence, adverse effects, and drug resistance [4,5]. Instead of focusing solely on conventional single-target therapies, recent research has turned to natural products and traditional medicines as potential complementary strategies, owing to their multi-target regulatory properties [6,7]. Extracts and bioactive compounds from these natural sources have shown the ability to modulate inflammatory pathways (e.g., TLR4/NF-κB) and regulate the gut microbiota [8–12]. However, high-quality clinical evidence for these natural products remains relatively scarce, and further preclinical evaluation is essential.

Among natural resources, medicinal fungi have garnered considerable attention. For instance, *Calvatia gigantea* possesses antibacterial and anti-inflammatory properties, and its extracts can accelerate wound healing by downregulating pro-inflammatory cytokines [13,14]. Additionally, protein extracts from *Calvatia lilacina* have demonstrated anti-cancer effects in vitro [15]. While extensive research has focused on the *Calvatia* genus, another genus within the fungal kingdom, *Scleroderma*, has also demonstrated promising anti-inflammatory potential. For example, ergosterol isolated from *Scleroderma polyrhizum* significantly reduced TNF-α and IL-6 levels in LPS-induced acute lung injury by inhibiting NF-κB activation [16]. Despite these findings, studies on the *Scleroderma bovista* species, particularly its fermentation broth, remain extremely scarce. Therefore, bridging the gap between the known anti-inflammatory properties of *Scleroderma* fungi and their potential application in IBD, we hypothesized that *S. bovista* fermentation broth (SBF) could exert alleviating effects on UC. To this end, the present study established an IBD inflammatory model [17] to systematically evaluate the anti-inflammatory effects of SBF and its potential mechanisms of action, with particular attention to its regulatory effects on the gut microbial community, thereby providing experimental evidence for the development and utilization of fungal resources from the genus Scleroderma.

2. Materials and Methods

2.1. Preparation of Fermentation Broth

S. bovista (a patented strain deposited in the China General Microbiological Culture Collection Center [CGMCC] under accession number CGMCC No. 40054) was inoculated onto potato dextrose agar (PDA) (Qingdao Hope Bio-Technology Co., Ltd., Qingdao, China) slants and incubated at 28 °C for 7 d for activation. Mycelial plugs (5 mm in diameter) were cut from the activated cultures using a sterile cork borer (Shanghai Qiaoxing Trading Co., Ltd., Shanghai, China) and transferred to 250 mL Erlenmeyer flasks containing 100 mL of basal Modified Melin-Norkrans (MMN) (Beijing Solarbio Science & Technology Co., Ltd., Beijing, China) liquid medium (three plugs per flask). The flasks were incubated at 28 °C and 150 r/min on a rotary shaker (Changzhou Jintan Jingda Instrument Manufacturing Co., Ltd., Changzhou, China) for 7 d to prepare the seed culture. For the final fermentation, 100 mL of medium in each 250 mL Erlenmeyer flask was inoculated with 5% (*v*/*v*) of the seed culture, followed by incubation in the dark at 28 °C and 150 r/min for 60 d. After cultivation, the fermentation broth was filtered through a 500-mesh sterile nylon screen (Beijing Solarbio Science & Technology Co., Ltd., Beijing, China) to remove the mycelia. The filtrate was concentrated to 1/30 of its original volume using a rotary evaporator (Zhengzhou

Bohui Precision Technology Co., Ltd., Zhengzhou, China) under reduced pressure at 40 °C in a water bath (Qingdao Jingcheng Instrument Co., Ltd., Qingdao, China). Finally, the concentrated broth was sterilized by filtration through a 0.22 μm microporous membrane (Yeasen Biotechnology Co., Ltd., Shanghai, China) under a laminar flow hood (Wuxi Xinbochen Environmental Protection Technology Co., Ltd., Wuxi, China). The resulting filtrate was designated as SBF concentrate and stored at 4 °C in the dark for subsequent experiments. The total dry solid content of the SBF concentrate was determined by drying 40 mL of the filtrate at 65 °C for 24 h, which yielded 0.4668 g of dry solids, corresponding to a concentration of 11.67 mg/mL. The concentrate was readily soluble in both distilled water and normal saline. The concentrate is a dark brown liquid with a pH of 5.7. For in vivo experiments, the administered doses (50, 100, and 200 mg/kg) were calculated based on this total dry solid mass, and the concentrate was fully dissolved in water or normal saline for oral gavage.

2.2. LC-MS/MS Analysis and Identification of SBF

An aliquot of 500 μL of the SBF was centrifuged at 13,000 rpm for 10 min, and the supernatant was collected for LC-MS/MS analysis using an UltiMate 3000 UHPLC system (Thermo Fisher Scientific, Waltham, MA, USA). Chromatographic separation was performed on a C18 column (1.9 μm, 2.1 mm × 100 mm) at a flow rate of 0.3 mL/min with an injection volume of 2 μL. The mobile phase consisted of 0.1% formic acid in water (A) and 0.1% formic acid in acetonitrile (B). The gradient elution program was as follows: 0–10 min, 90% A to 0% A (i.e., 10% B to 100% B); 10–15 min, 0% A (100% B); 15–17.1 min, 0% A to 90% A (100% B to 10% B); 17.1–20 min, 90% A (10% B).

The mass spectrometer was a Q-Exactive (Thermo Fisher Scientific, Waltham, MA, USA) equipped with a HESI source (Thermo Fisher Scientific, Waltham, MA, USA). The ion source temperature was set to 310 °C, capillary temperature to 320 °C, sheath gas flow rate to 30 arbitrary units, and auxiliary gas flow rate to 10 arbitrary units. The spray voltage was 3 kV in positive-ion mode and 2.8 kV in negative-ion mode.

Data-dependent acquisition (DDA) was employed for analysis, with a loop count of 10. Higher-energy collisional dissociation (HCD) was performed using step-wise normalized collision energies of 10, 28, and 35 eV. Full-scan MS1 spectra were acquired over a mass range of 100–1500 m/z at a resolution of 70,000, with an AGC target of 3E6 and a maximum injection time of 200 ms. MS2 spectra were acquired at a resolution of 17,500, with an AGC target of 1E5 and an injection time of 50 ms.

The raw data were processed using Compound Discoverer software (V3.2, Thermo Fisher Scientific, CA, USA). Database searches were performed against the mzCloud (2020B), bacterial metabolite, natural product, mzVault (2.3), metabolomics, and peptide databases. Compounds with higher abundance or higher match scores were retained, yielding a total of 43 compounds. To ensure batch-to-batch consistency and serve as a quality-control standard, the relative peak areas of the 13 most abundant constituents (Table 1) were monitored as a semi-quantitative chemical fingerprint for the SBF concentrate used in this study.

2.3. Cell Culture and Viability Assay

The RAW264.7 murine macrophage cell line (obtained from Jilin University, Changchun, China) was cultured in high-glucose Dulbecco's Modified Eagle Medium (DMEM; Thermo Fisher Scientific, Suzhou, China) supplemented with 10% fetal bovine serum (FBS; LONSA SCIENCE SRL, Canelones, Uruguay) and 1% penicillin-streptomycin (Beijing Lanmu Technology Co., Ltd., Beijing, China). Cells were maintained at 37 °C in a humidified incubator with 5% CO_2 and routinely passaged.

Table 1. The top 13 chemical constituents identified in *S. bovista* fermentation broth (SBF) by UHPLC-HR-MS/MS, ranked by descending peak area.

Compound Name	Molecular Formula	Molecular Weight	Retention Time (min)	Peak Area
Sclerocitrin homologs	$C_{34}H_{18}O_{14}$	650.07	8.17	6193809950
(Z)-N-15-carboxypentadec-9-enoyl-L-alanine methyl ester or isomers	$C_{20}H_{32}O_5$	369.25	6.145	2267719024
	$C_{11}H_{14}N_4O_2$	234.11	1.11	2004396258
	$C_{18}H_{31}ClN_4O_4$	402.20	6.894	1733187733
(Z)-N-15-carboxypentadec-9-enoyl-L-alanine methyl ester or isomers	$C_{20}H_{32}O_5$	369.25	6.387	1530666747
	$C_{12}H_8O_6$	248.03	4.61	1382750637
Cyclo-(L-Leu-L-Leu-L-Leu-L-Leu-L-Leu-L-Leu-L-Leu)	$C_{36}H_{66}N_6O_6$	678.50	5.882	983223347
Sclerocitrin	$C_{36}H_{22}O_{17}$	726.09	7.882	767822962
Cyclo-(L-Leu-L-Leu-L-Leu-L-Leu-L-Leu)	$C_{30}H_{55}N_5O_5$	565.42	5.529	653259141
lenticin	$C_{14}H_{18}N_2O_2$	246.14	3.174	612691452
Cyclo(phenylalanyl-prolyl)	$C1_4H_{16}N_2O_2$	244.12	5.604	557050471
3-[(4-hydroxyphenyl)methyl]-octahydropyrrolo[1,2-a]pyrazine-1,4-dione	$C_{14}H_{16}N_2O_3$	260.12	2.728	510555242
7,8-dimethylalloxazine (lumichrome)	$C_{12}H_{10}N_4O_2$	242.08	6.174	501402687

Cytotoxicity of SBF under normal conditions. The cytotoxicity of SBF against RAW264.7 cells was evaluated using a Cell Counting Kit-8 (CCK-8; Beyotime Biotechnology, Shanghai, China). Cells in the logarithmic growth phase were seeded into 96-well plates at a density of 1×10^3 cells/well (100 µL/well) and pre-incubated at 37 °C for 24 h to allow attachment. The supernatant was then removed and replaced with fresh medium containing SBF at various concentrations (5, 10, 20, and 40 µg/mL), with three replicate wells per concentration. A blank control group (medium only, no cells) and a negative control (NC) group (cells without SBF) were included. After an additional 24 h incubation, 10 µL of CCK-8 solution was added to each well, and the plates were incubated in the dark at 37 °C for 2 h. Absorbance at 450 nm (OD_{450}) was measured using a microplate reader (Tecan Austria GmbH, Grödig, Austria).

Cytotoxicity of SBF under LPS-stimulated conditions. To assess whether SBF affects the viability of inflammatory macrophages, RAW264.7 cells were seeded and attached as described above, then pretreated with SBF (5, 10, 20, 40 µg/mL) for 4 h, followed by stimulation with LPS (1 µg/mL) for 24 h. A blank control group (CON; no LPS, no SBF), a negative control group (NC; LPS-stimulated, no SBF), and SBF-treated groups (SBF5-SBF40; LPS-stimulated + SBF) were included, with three replicates each. Cell viability was then assessed using the CCK-8 assay as described above.

2.4. Nitric Oxide (NO) Production Assay

RAW264.7 cells in the logarithmic growth phase were seeded into 96-well plates at a density of 1×10^4 cells/well and cultured at 37 °C in a 5% CO_2 incubator for 24 h to allow attachment. After discarding the supernatant, cells were pretreated with fresh complete DMEM containing SBF (5, 10, 20, 40 µg/mL) for 4 h. A blank control group (CON; no LPS, no SBF) and a model control group (NC; LPS-stimulated, no SBF) were included, with three replicate wells per group. Following pretreatment, all groups except CON were stimulated

with LPS (Beyotime Biotechnology, Shanghai, China) (final concentration 1 μg/mL) for an additional 24 h to induce NO production. Culture supernatants were collected and mixed with Griess reagent (Beyotime Biotechnology, Shanghai, China) at a 1:1 volume ratio (50 μL supernatant + 50 μL Griess reagent). After incubation at room temperature in the dark for 10 min, absorbance at 540 nm (OD_{540}) was measured using a microplate reader.

2.5. Animal Study Design

Specific pathogen-free (SPF) male C57BL/6 mice, aged 6–8 weeks, were purchased from Liaoning Changsheng Biotechnology Co., Ltd. (Benxi, China) and acclimatized for one week under controlled conditions: temperature 22 ± 2 °C, relative humidity 50–60%, and a 12 h light/12 h dark cycle, with free access to food and water. Mice were randomly allocated using an Excel-generated random number sequence after acclimation.

All animal procedures were approved by the Ethics Committee of Jilin Normal University (Approval No.: KJLL20251002). The mice were randomly divided into six groups ($n = 6$ per group): CON (blank control), normal drinking water and daily oral gavage of normal saline (0.9% NaCl, 10 mL/kg); NC (negative control), 3% (w/v) DSS in drinking water and daily oral gavage of an equal volume of normal saline (0.9% NaCl, 10 mL/kg) by oral gavage; 5-ASA (positive control, Yeasen Biotechnology, Shanghai, China; Cat. No. 60317ES25), 3% DSS + daily oral gavage of 50 mg/kg 5-aminosalicylic acid; SBF50, SBF100, and SBF200 (treatment groups), 3% DSS + daily oral gavage of SBF at 50, 100, and 200 mg/kg of total dry solids, respectively. All agents were dissolved in normal saline (0.9% NaCl), which also served as the vehicle for the NC group. Except for the CON group, acute colitis was induced in all other groups by providing 3% (w/v) dextran sulfate sodium (DSS; MP Biomedicals, Irvine, CA, USA; Catalogue No. 160110; molecular weight 36–50 kDa) in drinking water from day 1 through day 8. This molecular weight range was selected because it is the standard grade widely used to induce reproducible acute colitis in mice. Simultaneously, the 5-ASA and SBF-treated groups received the corresponding agents (freshly prepared in normal saline daily) by daily oral gavage (10 mL/kg) over the same period. Body weight and disease activity index (DAI; based on body weight loss, fecal consistency, and rectal bleeding) were recorded daily [18]. Dosing personnel were necessarily aware of group assignment because each group received a different dose, and animal caretakers were not blinded; however, all outcome assessors were fully blinded to group allocation.

On day 8, all mice were euthanized by cervical dislocation, and colons were excised and measured for length. Spleens were harvested and weighed. Colon tissues were snap-frozen in liquid nitrogen or fixed in 4% paraformaldehyde (Shanghai Macklin Biochemical Technology Co., Ltd., Shanghai, China) for subsequent histological and molecular analyses. For all outcome assessments (DAI, gross appearance, histology, and IHC), animals and samples were re-coded with blinded IDs, and assessors were fully blinded to group allocation. No animals or data points were excluded, and all six mice per group were included in every endpoint, except for 16S rRNA sequencing (where $n = 3$ per group were selected due to strict sample quality control).

2.6. Histological Analysis and Colitis Scoring

On day 8, mice were euthanized and the entire colon was immediately excised. Colons were gently flushed with phosphate-buffered saline (PBS, pH 7.4) to remove fecal contents, and colon length was measured. Colonic tissues were then trimmed into 2–3 mm segments, fixed in 4% paraformaldehyde for at least 24 h, dehydrated through a graded ethanol series, cleared in xylene, and embedded in paraffin. Serial sections of 4 μm thickness were prepared using a microtome (Leica Biosystems Nussloch GmbH, Nussloch, Germany). For histological evaluation, sections were subjected to hematoxylin and eosin (H&E) staining.

Briefly, deparaffinized and rehydrated sections were stained with Harris hematoxylin (Beyotime Biotechnology, Shanghai, China) for 3–8 min, differentiated in 1% hydrochloric acid-ethanol for several seconds, blued in 0.6% ammonia water, and counterstained with eosin for 1–3 min. After dehydration and clearing, sections were mounted with neutral balsam (Sinopharm Chemical Reagent Co., Ltd., Shanghai, China). To assess macrophage infiltration, immunohistochemical (IHC) staining was performed using a rabbit anti-mouse F4/80 antibody (Cell Signaling Technology, Danvers, MA, USA) following standard protocols. The infiltration of F4/80+ cells was visually evaluated in three randomly selected fields per section under a light microscope (Leica Microsystems, Wetzlar, Germany).

2.7. Quantitative Real-Time Polymerase Chain Reaction (qRT-PCR)

Colonic tissue samples (approximately 0.3–0.5 cm × 0.3–0.5 cm) were collected from the rectal segment located 1–2 cm proximal to the anal verge. Total RNA was extracted using an RNA extraction kit (Aidlab Biotechnologies Co., Ltd., Beijing, China) and quantified using a UV-Vis spectrophotometer (Thermo Fisher Scientific, Waltham, MA, USA) to assess concentration and purity (A_{260}/A_{280} ratio). Subsequently, 1 μg of total RNA was reverse-transcribed into first-strand cDNA using random hexamer primers (Aidlab) and a reverse transcription kit (Aidlab), following the manufacturer's instructions. Real-time quantitative PCR (qPCR) was performed in a final volume of 20 μL containing 10 ng of cDNA template, 200 nM of each primer (forward and reverse), and 10 μL of 2 × SYBR Green qPCR Master Mix (Aidlab). Primer sequences are provided in Supplementary Table S1. The thermal cycling protocol comprised an initial denaturation at 95 °C for 30 s, followed by 40 cycles of 95 °C for 5 s and 60 °C for 30 s. Melting curve analysis was conducted after amplification to confirm product specificity. All reactions were run on an ABI QuantStudio 6 Flex Real-Time PCR System (Applied Biosystems, Thermo Fisher Scientific, Foster City, CA, USA). Relative mRNA expression levels were normalized to the endogenous reference gene *Gapdh* and calculated using the $2^{-\Delta\Delta Ct}$ method.

2.8. Western Blot Analysis

Total proteins were extracted from mouse colonic tissues using RIPA lysis buffer (KIGENE Biotech, Shanghai, China) supplemented with a protease/phosphatase/PMSF inhibitor cocktail (KIGENE Biotech). Protein concentrations were determined using a BCA Protein Assay Kit (KIGENE Biotech). Equal amounts of protein (20 μg per lane) were separated by SDS-PAGE using a rapid gel preparation kit (KIGENE Biotech) and subsequently transferred onto PVDF membranes (KIGENE Biotech) via wet transfer. After transfer, the membranes were blocked with 5% non-fat dry milk (Bio-Rad, Hercules, CA, USA) in TBST (Tris-buffered saline containing 0.1% Tween-20) for 2 h at room temperature. The membranes were then incubated overnight at 4 °C with primary antibodies against total IκBα, phosphorylated IκBα (p-IκBα), total p65, and phosphorylated p65 (p-p65) (KIGENE Biotech, Shanghai, China). Following three washes with TBST, the membranes were incubated with horseradish peroxidase (HRP)-conjugated secondary antibodies (Goat Anti-Rabbit IgG HRP; Goat Anti-Mouse IgG HRP; KIGENE Biotech) for 1 h at room temperature. Immunoreactive bands were visualized using an enhanced chemiluminescence (ECL) substrate (KIGENE Biotech) and imaged with a gel documentation system (Tanon 4600, Shanghai, China). Relative protein levels were quantified using ImageJ software (version 1.53, National Institutes of Health, Bethesda, MD, USA). For NF-κB pathway analysis, the ratios of p-IκBα/total IκBα and p-p65/total p65 were calculated, with β-actin (KIGENE Biotech) as the loading control.

2.9. Enzyme-Linked Immunosorbent Assay

Mouse colonic tissues were rinsed with ice-cold PBS to remove fecal contents, weighed, and homogenized in PBS using a tissue homogenizer (Wuhan Servicebio Technology Co., Ltd., Wuhan; China) at 10,000–15,000 rpm to prepare 10% (w/v) tissue homogenates. The homogenates were centrifuged at ~1000× g for 10–15 min, and the supernatants were collected. The levels of tumor necrosis factor-α (TNF-α), interleukin-1β (IL-1β), interleukin-6 (IL-6), and interleukin-10 (IL-10) in the colonic tissue homogenates were quantified using commercial ELISA kits (Shanghai Yixiu Biotechnology, Shanghai, China) strictly following the manufacturer's instructions. After the reaction, the absorbance of each well was measured at 450 nm using a microplate reader, and cytokine concentrations were calculated from standard curves.

2.10. 16S rRNA Gene Sequencing and Taxonomic Assignment

Following DSS induction and SBF treatment, fecal samples were collected from mice on day 8. Although samples were collected from all six mice per group, strict quality control criteria (e.g., sufficient genomic DNA yield and optimal sequencing depth) were applied during library preparation. Consequently, high-quality samples from three mice per group ($n = 3$) were selected for final 16S rRNA sequencing analysis to ensure data reliability. Total genomic DNA was extracted using the FastPure Stool DNA Isolation Kit (MJYH, Shanghai, China), and DNA quality and concentration were assessed by agarose gel electrophoresis and NanoDrop spectrophotometry (Thermo Fisher Scientific, Waltham, MA, USA). The V3-V4 hypervariable regions of the bacterial 16S rRNA gene were amplified with barcoded primers 338F (5′-ACTCCTACGGGAGGCAGCAG-3′) and 806R (5′-GGACTACHVGGGTWTCTAAT-3′). The PCR protocol consisted of initial denaturation at 95 °C for 3 min, followed by 27 cycles of 95 °C for 30 s, 55 °C for 30 s, and 72 °C for 30 s, with a final extension at 72 °C for 10 min. Amplicons were purified and used to construct paired-end sequencing libraries, which were sequenced on an Illumina NextSeq 2000 platform (Illumina, Inc., San Diego, CA, USA).

Raw sequence data were quality-filtered using fastp and assembled with FLASH (minimum overlap 10 bp, maximum mismatch rate 0.2). Amplicon sequence variants (ASVs) were inferred by denoising with DADA2 (v2020.2) within QIIME2 (v2020.2); chloroplast and mitochondrial sequences were removed. All samples were rarefied to 20,000 sequences per sample for downstream analyses. Taxonomic annotation was performed using a Naive Bayes classifier trained on the SILVA release 138 database. Alpha diversity was evaluated by the Shannon index, and beta diversity was assessed by principal coordinate analysis (PCoA) based on weighted UniFrac distances at the ASV level. Differentially abundant taxa among groups were identified using the Linear Discriminant Analysis Effect Size (LEfSe) method on the Galaxy platform (version 1.0). Community compositional patterns were further visualized by genus-level heatmaps and bar plots. The data have been deposited in the NCBI BioProject database under accession number PRJNA1532645 (https://www.ncbi.nlm.nih.gov/bioproject/PRJNA1532645, accessed on 21 September 2026).

Raw sequence data were quality-filtered using fastp (v0.20.0) and assembled with FLASH (v1.2.11). ASVs were inferred by denoising with DADA2 within QIIME2 (v2020.2). All samples were rarefied to 20,000 sequences. Alpha diversity was evaluated by the Shannon index, and differences among groups were compared using the Kruskal–Wallis test followed by Dunn's multiple comparisons test. Beta diversity was assessed by PCoA based on weighted UniFrac distances, and statistical significance was evaluated by PERMANOVA (adonis2) with $R^2 = 0.6397$ and $p = 0.001$. LEfSe was performed with an LDA threshold > 2.0.

2.11. Statistical Analyses

Data analyses were conducted using SPSS (version 27.0) and GraphPad Prism (version 10.0). For in vitro assays, data are presented as mean ± SEM from at least three independent biological replicates. For in vivo continuous data, data are presented as mean ± SEM ($n = 6$ mice/group) and analyzed by One-way ANOVA followed by Tukey's or Dunnett's multiple comparisons test. For ordinal data (e.g., DAI scores, histological scores), Kruskal–Wallis tests followed by Dunn's multiple comparisons test were used. A p-value < 0.05 was considered statistically significant.

3. Results

3.1. Chemical Profiling of SBF by LC-MS Analysis

High-resolution liquid chromatography-mass spectrometry (HR-LC-MS) was employed to analyze the chemical constituents of *S. bovista* concentrated broth (SBF) in both positive-ion (Figure 1A) and negative-ion (Figure 1B) modes. The total ion current intensities were 5.84×10^8 and 1.36×10^8 in positive and negative modes, respectively, with prominent chromatographic peaks distributed across the 0.7–19.0 min retention time window. Based on accurate mass measurements and database matching, a total of 43 major constituents were identified from SBF (Table S2). The thirteen most abundant compounds, ranked by peak area, are summarized in Table 1. To ensure batch-to-batch consistency and to serve as a quality-control standard, the relative peak areas of the 13 most abundant constituents (Table 1) were monitored as a quantitative chemical fingerprint for the SBF concentrate used in this study. All in vitro and in vivo experiments reported here were performed with a single large-scale fermentation batch, thereby ensuring internal consistency across assays. Six of these were subsequently isolated for structural confirmation (Figure S1). The identified compounds spanned multiple structural classes, including sclerocitrin and its homologues (e.g., $C_{34}H_{18}O_{14}$, RT = 8.17 min; $C_{36}H_{22}O_{17}$, RT = 7.88 min), cyclic peptides (e.g., $C_{36}H_{66}N_6O_6$, RT = 5.88 min; $C_{30}H_{55}N_5O_5$, RT = 5.53 min), alkaloids such as hypaphorine ($C_{14}H_{18}N_2O_2$, RT = 3.17 min) and 3-[(4-hydroxyphenyl)methyl]octahydropyrrolo[1,2-a]pyrazine-1,4-dione ($C_{14}H_{16}N_2O_3$, RT = 2.73 min), long-chain fatty acid derivatives (e.g., (Z)-*N*-15-carboxypentadec-9-enoyl-L-alanine methyl ester isomers, RT = 6.15 and 6.39 min), a chlorinated compound ($C_{10}H_{13}ClN_4O_4$, RT = 6.89 min), and 7,8-dimethylalloxazine (RT = 6.17 min). Collectively, these results demonstrate that SBF is chemically diverse, enriched in steroidal derivatives, cyclic peptides, alkaloids, and polar polypeptides—providing a foundation for elucidating its pharmacologically active material basis.

Among the identified constituents, sclerocitrin and its homologues were the most abundant (Table 1), consistent with previous reports of their antitumor and broad-spectrum antimicrobial activities, including against multidrug-resistant strains [19]. Notably, multiple cyclic peptides were detected in SBF. Compared with their linear counterparts, cyclic peptides possess constrained conformations, superior biochemical stability, enhanced membrane permeability, and resistance to proteolytic degradation—properties that have attracted considerable interest in anti-inflammatory and anticancer drug development [20]. For example, cyclic dipeptides derived from deep-sea bacteria have demonstrated both anticancer and immunomodulatory potential [21]. Furthermore, the alkaloid hypaphorine identified herein has been reported to alleviate LPS-induced inflammation via inactivating the NF-κB and ERK pathways in RAW264.7 macrophages [22].

Given that cyclic peptides and alkaloids with anti-inflammatory properties were prominently represented in SBF, it is reasonable to postulate that SBF may exert therapeutic effects on ulcerative colitis (UC). This chemical evidence provides a rationale for the subsequent in vivo and in vitro pharmacological evaluations.

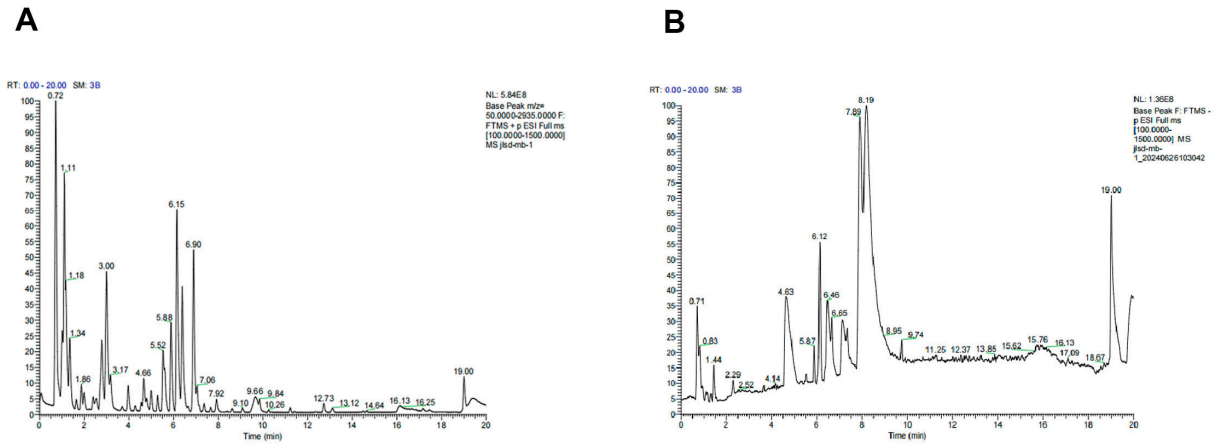


Figure 1. Base peak chromatograms (BPCs) of *S. bovista* fermentation broth (SBF) analyzed by UHPLC-HR-MS. (**A**) BPC in positive-ion mode; (**B**) BPC in negative-ion mode.

3.2. Anti-Inflammatory Effects of SBF on LPS-Stimulated RAW264.7 Macrophages

We first evaluated the effect of SBF on the viability of normal RAW264.7 macrophages using the CCK-8 assay (Figure 2A). Treatment with SBF at 5, 10, 20, and 40 μg/mL for 24 h significantly enhanced cell viability compared with the blank control (CON) group ($p < 0.05$ for all concentrations), indicating that SBF promotes macrophage viability in a concentration-dependent manner. Notably, the SBF20 and SBF40 groups showed significantly higher viability than the SBF5 and SBF10 groups ($p < 0.05$), while no significant difference was observed between SBF20 and SBF40, nor between SBF5 and SBF10. These results demonstrate that SBF is not only non-cytotoxic but also exerts a pro-viability effect on RAW264.7 cells within the tested concentration range, with 20 μg/mL representing the threshold concentration for maximal viability stimulation.

To further assess the protective effect of SBF against inflammatory damage, an in vitro inflammatory model was established by stimulating RAW264.7 cells with LPS (1 μg/mL) for 24 h. As shown in Figure 2B, LPS stimulation drastically reduced cell viability to 45.0% of the blank control (CON, no LPS/no SBF) level ($p < 0.001$), confirming successful induction of inflammatory injury. Pretreatment with SBF (5–40 μg/mL) for 4 h prior to LPS challenge restored cell viability in a concentration-dependent manner, with the 40 μg/mL group recovering to near-normal levels ($p < 0.01$ vs. NC).

We next measured the production of nitric oxide (NO), a key pro-inflammatory mediator. As shown in Figure 2C, LPS stimulation markedly elevated NO release from the CON level to approximately 10-fold higher in the NC group. SBF pretreatment dose-dependently suppressed LPS-induced NO overproduction, with the 40 μg/mL group reducing NO levels by ~49% compared with NC ($p < 0.01$).

To elucidate the molecular basis of SBF-mediated anti-inflammatory effects, we examined the mRNA expression of inflammation-related genes by RT-qPCR (Figure 2D–G). LPS stimulation profoundly upregulated the expression of pro-inflammatory genes *iNOS* (Figure 2D), *IL-1β* (Figure 2E), and *COX-2* (Figure 2F) compared with CON. SBF pretreatment (5–40 μg/mL) significantly downregulated the mRNA levels of all three genes in a concentration-dependent fashion, with the 40 μg/mL group showing reductions of 6-fold, 5-fold, and 1.7-fold for *iNOS*, *IL-1β*, and *COX-2*, respectively (all $p < 0.01$ vs. NC). Conversely, LPS suppressed the expression of the anti-inflammatory cytokine *IL-10* (Figure 2G), and SBF pretreatment restored *IL-10* mRNA levels in a dose-dependent manner, reaching an 8.5-fold increase at 40 μg/mL ($p < 0.01$ vs. NC).

Collectively, these in vitro results demonstrate that SBF confers potent protection against LPS-induced inflammatory injury in RAW264.7 macrophages. At the cellular level,

SBF not only enhanced basal macrophage viability in a concentration-dependent manner but also reversed LPS-induced viability loss. At the molecular level, SBF suppressed the production of the key pro-inflammatory mediator NO and downregulated the expression of pro-inflammatory genes *iNOS*, *IL-1β*, and *COX-2*, while concomitantly restoring the expression of the anti-inflammatory cytokine *IL-10*. These findings establish a clear in vitro proof-of-concept that SBF exerts multi-target anti-inflammatory activity, providing a mechanistic rationale for its subsequent evaluation in a DSS-induced colitis mouse model.

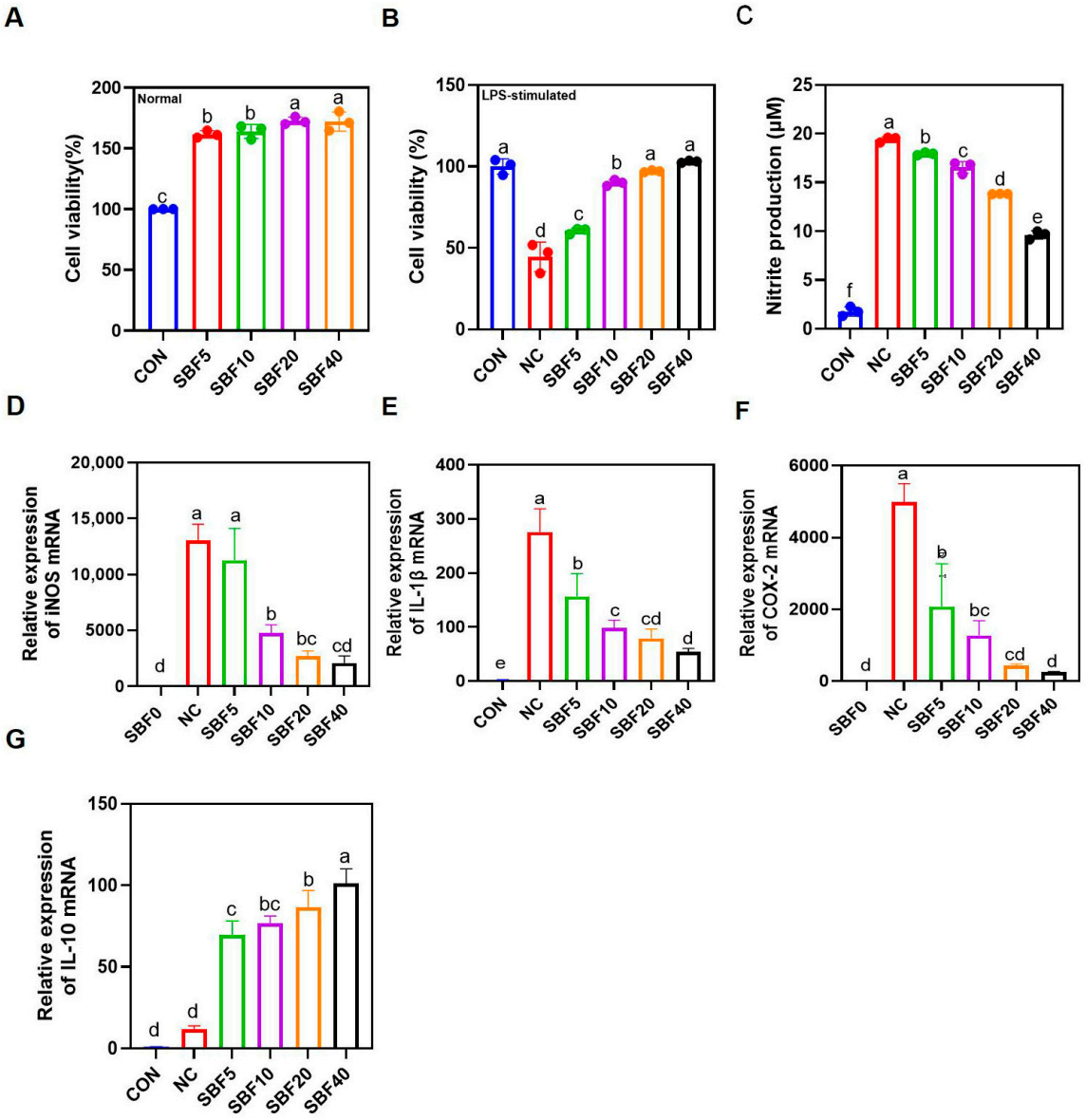


Figure 2. Effects of SBF on RAW264.7 macrophage viability and LPS-induced inflammatory responses. (**A**) Viability of normal RAW264.7 cells treated with SBF (5, 10, 20, 40 μg/mL) for 24 h, assessed by CCK-8 assay. (**B**) Viability of LPS-stimulated RAW264.7 cells pretreated with SBF (5–40 μg/mL), assessed by CCK-8 assay. (**C**) NO production in LPS-stimulated RAW264.7 cells pretreated with SBF, measured by Griess assay. (**D**–**G**) Relative mRNA expression levels of *iNOS* (**D**), *IL-1β* (**E**), *COX-2* (**F**), and *IL-10* (**G**) in LPS-stimulated RAW264.7 cells treated with SBF, determined by RT-qPCR. CON, blank control (no LPS, no SBF); NC, negative control (LPS-stimulated, no SBF); SBF5-SBF40, LPS-stimulated cells treated with 5–40 μg/mL SBF. Data are mean ± SD ($n = 3$). Different lowercase letters above bars indicate significant differences ($p < 0.05$).

3.3. Protective Effects of SBF on DSS-Induced Ulcerative Colitis in Mice

To evaluate the in vivo anti-inflammatory activity of SBF, a 3% DSS-induced mouse model of ulcerative colitis was employed (Figure 3). As shown in Figure 3A, mice in the NC group began to lose body weight from day 5 post-induction, with a significant reduction by day 8 compared with the CON group, accompanied by typical colitic symptoms including diarrhea and hematochezia, indicating successful establishment of the colitis model. Both 5-ASA (50 mg/kg) and SBF treatments (50–200 mg/kg) alleviated body weight loss in a dose-dependent manner (Figure 3B).

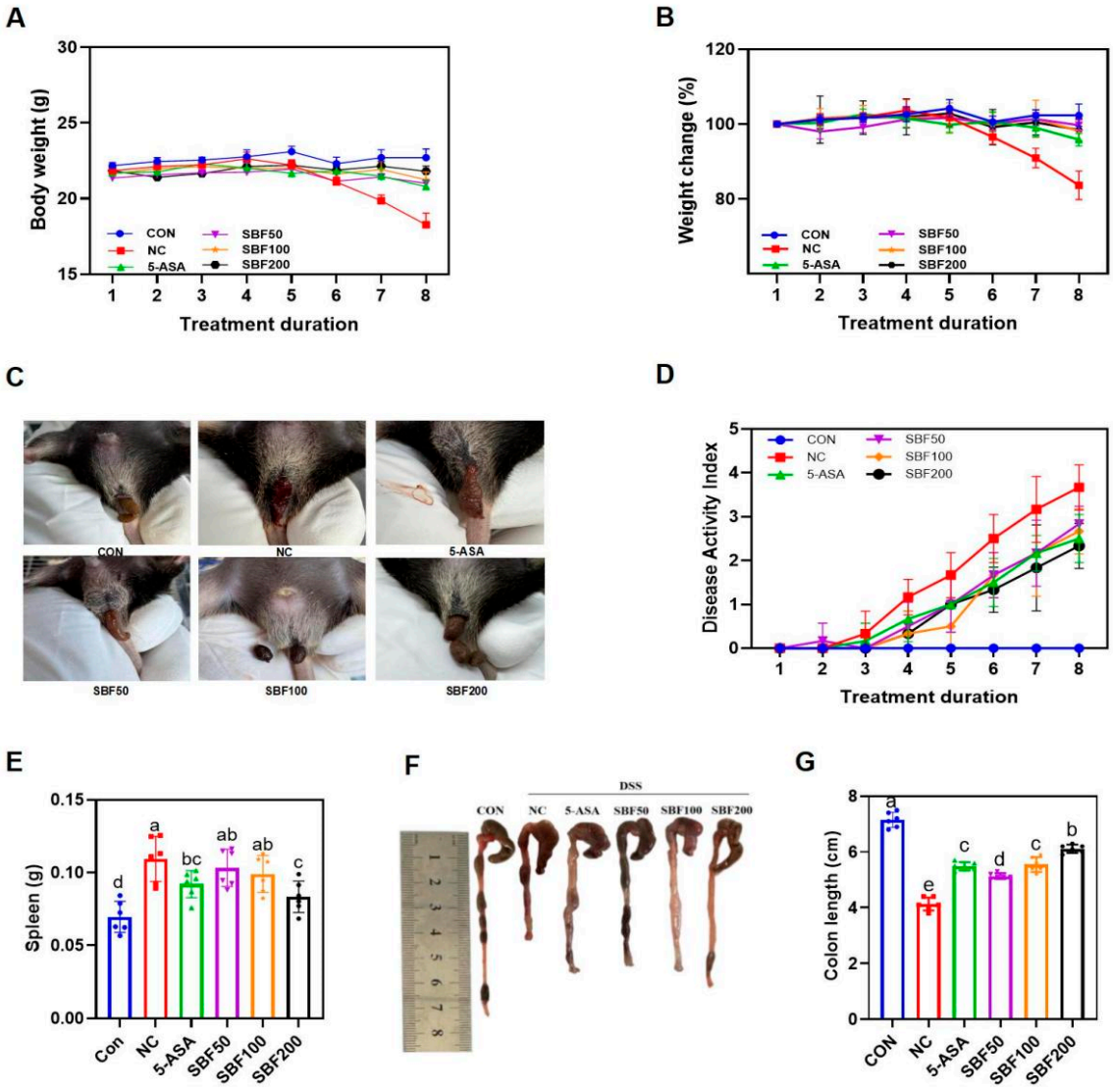


Figure 3. Protective effects of SBF on DSS-induced acute colitis in mice. (**A**) Dynamic body weight changes during the 8-day experimental period; (**B**) percentage body weight change on day 8; (**C**) representative photographs of anal appearance and fecal characteristics on day 8; (**D**) disease activity index (DAI) scores from days 1 to 8; (**E**) spleen weight on day 8; (**F**) representative photographs of excised colons on day 8; (**G**) colon length on day 8. CON, blank control (normal drinking water, no DSS, no treatment); NC, model control (3% DSS in drinking water, treated with equal volume of normal saline); 5-ASA, positive control (3% DSS + 50 mg/kg 5-aminosalicylic acid); SBF50, SBF100, and SBF200, treatment groups (3% DSS + SBF at 50, 100, and 200 mg/kg, respectively). Data are mean ± SEM ($n = 6$). Bars sharing different lowercase letters indicate significant differences ($p < 0.05$).

The severity of diarrhea and hematochezia was visually assessed on day 8 (Figure 3C). NC mice exhibited severe rectal bleeding and loose stools, whereas SBF100 and SBF200 groups displayed markedly reduced fecal blood and improved stool consistency, approaching the appearance of CON mice. The disease activity index (DAI) scores (Figure 3D) were markedly elevated in the NC group relative to CON. Compared with NC, both 5-ASA and all three SBF doses (50, 100, and 200 mg/kg) lowered the DAI scores to varying degrees. SBF200 showed the most pronounced reduction among the three doses, approaching the level of the 5-ASA group.

Spleen weight (Figure 3E), a systemic indicator of inflammation, was significantly increased in NC mice compared with CON ($p < 0.001$), suggesting excessive splenic immune activation. SBF intervention dose-dependently inhibited spleen enlargement, with SBF200 reducing spleen weight to near-CON levels and outperforming 5-ASA.

Colon length shortening is a characteristic pathological change in DSS-induced colitis. As shown in Figure 3F,G, the NC group exhibited marked colon shortening compared with CON ($p < 0.001$). SBF treatment significantly ameliorated colon shortening in a dose-dependent fashion ($p < 0.01$ for SBF100 and SBF200 vs. NC). Notably, colon length increased progressively with ascending SBF dose, and significant differences were detected between every pair of adjacent SBF concentrations (SBF50 vs. SBF100, SBF100 vs. SBF200; all $p < 0.05$). Furthermore, the SBF200 group restored colon length to levels indistinguishable from CON and showed significantly better preservation than 5-ASA ($p < 0.05$), indicating that SBF effectively alleviates DSS-induced colonic tissue injury.

Collectively, these in vivo results demonstrate that SBF exerts a potent protective effect against DSS-induced ulcerative colitis, with SBF200 (200 mg/kg) matching or surpassing the efficacy of the clinically used drug 5-ASA across multiple phenotypic endpoints—including body weight preservation, DAI reduction, suppression of splenomegaly, and rescue of colon length. The dose-dependent restoration of colon length, in particular, reveals a clear SBF concentration-response relationship and identifies 200 mg/kg as the optimal therapeutic dose, providing a strong rationale for further investigation into the gut microbiota-mediated mechanisms underlying SBF's superior efficacy.

3.4. Effects of SBF on DSS-Induced Colonic Tissue Injury and the NF-κB Signaling Pathway

H&E staining was employed to evaluate the protective effect of SBF against colonic histopathological damage. The results (Figure 4A) showed that the distal colon of mice in the DSS model group exhibited pronounced disruption of mucosal architecture, loss of crypts, and extensive inflammatory cell infiltration. Compared with the model group, SBF intervention markedly attenuated these pathological changes in a dose-dependent manner, with gradual preservation of crypt structure and reduced inflammatory cell infiltration observed at higher doses.

ELISA was performed to quantify inflammatory cytokine levels in colonic tissues. Compared with the model group, SBF treatment significantly decreased the levels of pro-inflammatory cytokines *IL-1β* (Figure 4B), *TNF-α* (Figure 4C), and *IL-6* (Figure 4D) in a dose-dependent manner ($p < 0.05$). Notably, at the highest dose (SBF200), the levels of these three cytokines were reduced to values comparable to those of the 5-ASA-treated group, with no significant differences observed between SBF200 and 5-ASA ($p \geq 0.05$). Interestingly, all three SBF-treated groups exhibited significantly lower *IL-10* levels (Figure 4E) than the 5-ASA group ($p < 0.05$), suggesting that SBF suppresses colonic inflammation through a distinct immunomodulatory profile compared with the conventional aminosalicylate. These findings indicate that SBF exerts a dose-dependent regulatory effect on local colonic inflammation, with its high-dose efficacy approaching that of the positive control 5-ASA.

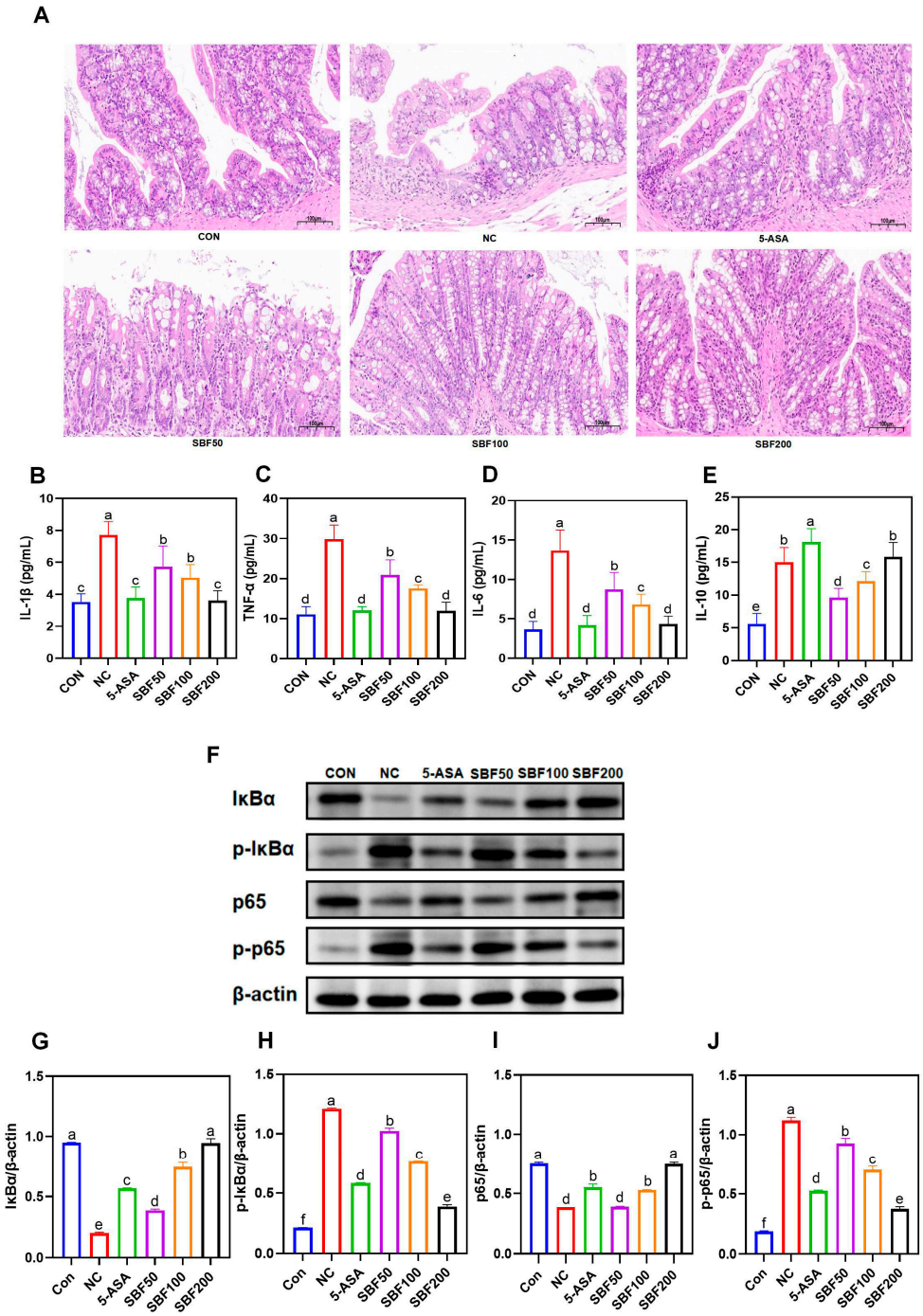


Figure 4. Effects of SBF on colonic histopathology, inflammatory cytokine production, and NF-κB signaling pathway in DSS-induced colitis mice. (**A**) Representative H&E-stained sections of colonic tissues; (**B**–**E**) Levels of *IL-1β* (**B**), *TNF-α* (**C**), *IL-6* (**D**), and *IL-10* (**E**) in colonic tissues, quantified by ELISA and normalized to tissue weight (pg/mg); (**F**) representative Western blot images showing protein expression of total IκBα, phosphorylated IκBα (p-IκBα), 65, and phosphorylated 65 (p-65); (**G**–**J**) Relative expression levels of IκBα, p-IκBα, p65, and p-p65 normalized to β-actin. CON, blank control (normal drinking water, no DSS); NC, model control (3% DSS in drinking water, no treatment); 5-ASA, positive control (3% DSS + 50 mg/kg 5-aminosalicylic acid); SBF50, SBF100, and SBF200, treatment groups (3% DSS + SBF at 50, 100, and 200 mg/kg, respectively). Data are mean ± SEM ($n = 6$). Bars sharing different lowercase letters indicate significant differences ($p < 0.05$).

To further investigate the anti-inflammatory mechanism of SBF, we examined the expression of key proteins in the NF-κB signaling pathway in colonic tissues by Western blot. As shown in Figure 4F–J, compared with the Con group, the NC group exhibited no significant change in total p65 expression, but showed elevated p-p65/p65 ratio, accompanied by elevated levels of phosphorylated IκBα (p-IκBα) and phosphorylated p65 (p-p65), indicating activation of the NF-κB pathway. Compared with the NC group, 5-ASA treatment significantly increased the expression of IκBα and p65 while decreasing the levels of p-IκBα and p-p65. Furthermore, compared with the 5-ASA group, SBF200 treatment resulted in even higher expression of IκBα and p65 and lower levels of p-IκBα and p-p65. These results demonstrate that SBF inhibits the excessive activation of the NF-κB signaling pathway in a dose-dependent manner.

Collectively, these findings demonstrate that SBF effectively alleviates DSS-induced colonic histopathological damage and dose-dependently modulates local inflammatory cytokine production, with its underlying mechanism involving suppression of NF-κB signaling pathway activation. The improvements in colonic tissue integrity and local inflammatory status are consistent with the observed modulation of gut microbiota composition, as detailed below.

3.5. Effects of SBF on Inflammatory Responses in DSS-Induced Colitic Mice

To further evaluate the anti-inflammatory effects of SBF in the DSS-induced colitis model, we assessed macrophage infiltration and related inflammatory indices in colonic tissues. F4/80 is a well-established marker for murine macrophages, and quantification of $F4/80^+$ cells enables evaluation of colonic inflammation severity and therapeutic efficacy. Immunohistochemical staining (Figure 5A) revealed sparse $F4/80^+$ macrophages in the colon of the CON group, whereas the DSS model group (NC) exhibited markedly increased macrophage infiltration with intensified staining. Representative immunohistochemical images suggested that SBF treatment attenuated macrophage infiltration, with the SBF200 group showing the most pronounced reduction in both cell number and staining intensity, indicating effective suppression of the inflammatory response. Concurrently, RT-qPCR analysis (Figure 5B–G) demonstrated that the mRNA expression levels of the pro-inflammatory cytokines *TNF*-α (Figure 5B), *IL*-6 (Figure 5C), *IL-1β* (Figure 5D), and *IFN*-γ (Figure 5E), the inflammatory enzyme *COX*-2 (Figure 5F), and the chemokine *MCP*-1 (Figure 5G) were all significantly elevated in the colonic tissues of the model group compared with the CON group ($p < 0.05$). SBF treatment dose-dependently downregulated the expression of these genes ($p < 0.05$), with the highest dose (SBF200) achieving reductions comparable to those of the 5-ASA-positive control.

Collectively, these findings indicate that SBF alleviates colonic tissue inflammation in DSS-induced colitis by suppressing macrophage infiltration and the associated network of pro-inflammatory cytokines, chemokines, and inflammatory mediators.

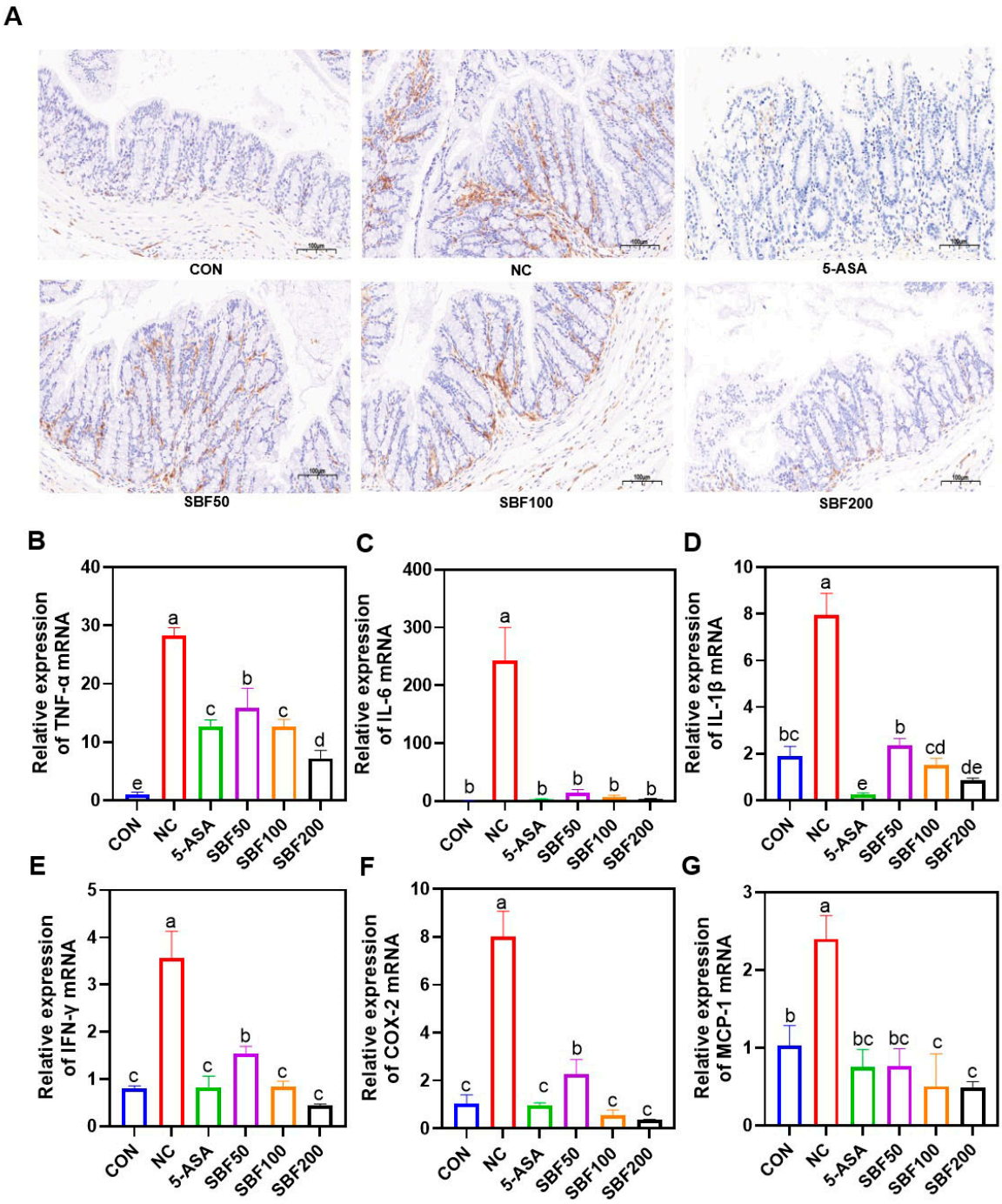


Figure 5. Effects of SBF on the inflammatory response in colonic tissues of mice with DSS-induced colitis. (**A**) Representative images of F4/80 immunohistochemical staining in mouse colon tissues after 7 days of DSS treatment; (**B**–**G**) Relative mRNA expression levels of inflammation-related genes, including *TNF-α* (**B**), *IL-6* (**C**), *IL-1β* (**D**), *IFN-γ* (**E**), *COX-2* (**F**), and *MCP-1* (**G**), in colon tissues as determined by quantitative real-time PCR (qPCR). CON, blank control group (normal drinking water); NC, model control group (free access to 3% DSS drinking water, without drug treatment); 5-ASA, positive drug control group (free access to 3% DSS drinking water, treated with 50 mg/kg 5-aminosalicylic acid); SBF50, SBF100, and SBF200 represent groups given free access to 3% DSS drinking water and treated with 50, 100, and 200 mg/kg SBF, respectively. Data are presented as the mean ± standard error of the mean (SEM). Different lowercase letters above the bars indicate statistically significant differences among groups ($p < 0.05$).

3.6. Changes in Gut Microbiota Following SBF Treatment in DSS-Induced Colitic Mice

To investigate the modulatory effects of SBF on the gut microbiota in DSS-induced ulcerative colitis mice, fecal microbial communities from each group were analyzed by 16S rRNA high-throughput sequencing. Alpha diversity, beta diversity, species composition, and differentially abundant taxa among groups were assessed. The alpha diversity results (Figure 6A) showed that the Shannon index in the NC model group was significantly elevated compared with the CON group. Notably, in the context of DSS-induced colitis, an elevated Shannon index in this model has been attributed to the expansion of taxa such as *Escherichia-Shigella* rather than to a healthier community. Intervention with 5-ASA did not reverse this trend, whereas SBF treatment (50, 100, and 200 mg/kg) markedly reduced the Shannon index back toward the CON level, indicating the suppression of these taxa and the restoration of a community structure closer to that of CON.

Consistent with this, principal coordinate analysis (PCoA) based on ASV-level weighted UniFrac distances (Figure 6B) showed that CON samples clustered tightly and were clearly separated from the NC group, indicating that DSS markedly altered the overall gut microbiota structure. While the 5-ASA group clustered close to the NC group, the SBF-treated groups (especially SBF100 and SBF200) shifted toward the CON cluster, with samples within each dose group showing relatively tight clustering. These results suggest that SBF specifically reshaped the gut microbiota structure, reversing the DSS-induced dysbiosis by counteracting the expansion of these taxa and promoting community normalization.

The genus-level community heatmap (Figure 6C) showed that DSS administration markedly altered the overall abundance patterns of the gut microbiota, as evidenced by the clear clustering separation between the NC and CON groups. SBF intervention reshaped these profiles, with the SBF100 and SBF200 groups clustering more closely to CON and exhibiting partial normalization of DSS-disrupted genera (e.g., *Clostridium*, *Escherichia-Shigella*, *Faecalibaculum*), whereas the 5-ASA group displayed only a modest restorative effect. LEfSe cladogram analysis (Figure 6D) identified distinct taxonomic signatures among groups, with the NC group showing significant expansion of *Escherichia-Shigella* (family Enterobacteriaceae) and *Thomasclavelia* (family Erysipelotrichaceae) at multiple phylogenetic levels. In contrast, SBF-treated groups exhibited increased abundance of taxa such as *Bifidobacterium* (order Bifidobacteriales) and *Christensenella*, suggesting that SBF reshaped the gut microbial hierarchy in DSS-induced dysbiosis.

The community barplot of dominant genera (Figure 6E) revealed distinct microbial compositional patterns among groups, with the NC group characterized by high relative abundances of *Clostridium*, *Akkermansia*, and *Escherichia-Shigella*, and the CON group dominated by *Dubosiella* and *Faecalibaculum*. SBF intervention, particularly at 100 and 200 mg/kg, markedly reduced the increased relative abundance of *Clostridium* and *Escherichia-Shigella* while promoting the relative abundance of *Dubosiella* (relative to NC). Consistently, among the genera whose abundance was increased following SBF treatment, *Akkermansia* and *Faecalibaculum* were markedly enriched in the SBF groups compared with the NC group (Figure 6F, G). Across all SBF dose groups, *Ligilactobacillus* relative abundance increased to varying degrees compared with the NC group, yet remained below CON levels (Figure 6H). Conversely, the three genera whose abundance was most reduced by SBF treatment—*Turicibacter*, *Clostridium*, and *Enterococcus*—were elevated in the NC group (with *Clostridium* also high in the 5-ASA group) and were significantly suppressed in the SBF50, SBF100, and SBF200 groups (Figure 6I–K), indicating that SBF effectively reversed the DSS-induced expansion of these taxa.

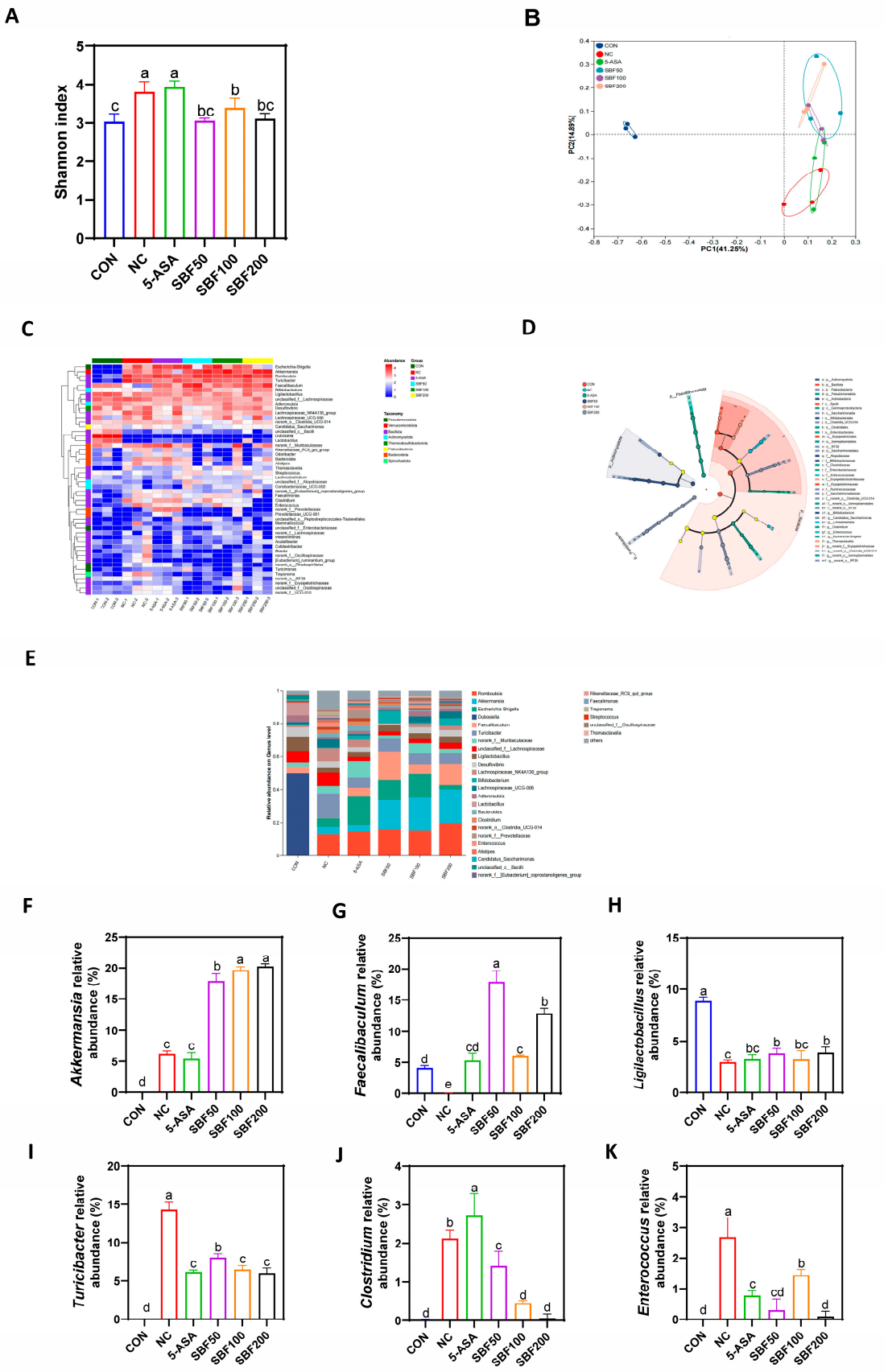


Figure 6. SBF modulates gut microbiota in DSS-induced colitis mice. (**A**) Shannon index; (**B**) Principal coordinate analysis (PCoA) based on weighted UniFrac distances at the ASV level; different colors/shapes indicate groups, and closer points suggest similar composition; (**C**) Genus-level heatmap

showing relative abundance; (**D**) Cladogram; (**E**) Community barplot displaying compositional distribution of dominant genera; (**F**–**H**) Top three bacterial genera with increased relative abundance after SBF treatment; (**I**–**K**) Top three bacterial genera with decreased relative abundance after SBF treatment. Group abbreviations: CON, blank control group (normal drinking water, no DSS); NC, model control group (3% DSS in drinking water, no drug); 5-ASA, positive control group (3% DSS water + 50 mg/kg 5-aminosalicylic acid); SBF50, SBF100, and SBF200, groups receiving 3% DSS water + SBF at 50, 100, and 200 mg/kg, respectively. Data are presented as mean ± standard error of the mean (SEM), $n = 3$. Different lowercase letters above bars indicate statistically significant differences among groups ($p < 0.05$).

4. Discussion

4.1. Chemical Diversity of SBF Provides a Multi-Target Pharmacological Basis

LC-MS/MS identified 43 bioactive constituents in SBF—sclerocitrin homologs, cyclic peptides, and alkaloids—typical of medicinal-fungus fermentation broths [23,24]. This diversity is therapeutically advantageous in UC, where single-target drugs fail against multifactorial pathogenesis [25,26]. Sclerocitrin-type pigments exhibit antimicrobial and antitumor activities [27,28]; cyclic peptides enable intracellular target engagement via conformational stability and membrane permeability [29,30]); alkaloids such as hypaphorine directly suppress inflammatory transcription [22,31]. Their co-occurrence embodies "multi-component synergy" and underpins SBF's concurrent inhibition of NO, IL-1β, and COX-2 alongside IL-10 restoration in LPS-stimulated macrophages (Figure 2). Fermentation enriches low-molecular-weight peptidic and phenolic species absent from the fruiting body, explaining dose-dependent colon-length rescue and comparable to 5-ASA at 200 mg/kg in this acute model (Figure 3). This chemical breadth maps onto downstream NF-κB inhibition and gut microbiota remodeling, consistent with the 43-compound pool contributing to SBF's integrated efficacy.

4.2. SBF Protects Macrophages from LPS-Induced Injury and Rebalances Inflammatory Mediators In Vitro

SBF protected RAW264.7 macrophages from LPS-induced injury, suppressed NO overproduction, and rebalanced pro-/anti-inflammatory gene expression. It exhibited dual cellular effects—promoting basal viability while reversing LPS-triggered viability loss—consistent with the non-toxic profile of *S. bovista* fermentation concentrates. Dose-dependent attenuation of *Nos2* (*iNOS*), *Il1b* (*IL-1β*), and *Ptgs2* (*COX-2*) transcription and restoration of *Il10(IL-10)* mRNA (Figure 2) aligned with NF-κB's role as the central switch governing iNOS/COX-2 expression. Given that 5-ASA alleviates colitis partly by blocking NF-κB nuclear translocation [32], SBF's parallel suppression of multiple mediators strongly implies an NF-κB-interfering mechanism. Downregulation of *Mcp1* further suggests dampened chemokine-driven monocyte recruitment [33]. Compared with anti-TNF-α biologics (primary non-response in ~30%) [34], SBF's multi-gene modulation reflects the advantage of multi-component natural formulations in refractory UC. Notably, endotoxin contamination is unlikely to account for these effects: SBF was applied at 5–40 μg/mL, whereas LPS was used at 1 μg/mL for stimulation, and any endotoxin present would be expected to promote rather than suppress inflammatory activation—the opposite of the pattern observed here (Figure 2C–G). In addition, SBF was derived from a pure culture of the deposited strain (CGMCC No. 40054) and sterilized through a 0.22 μm membrane, which minimizes the risk of Gram-negative contamination.

4.3. SBF Attenuates the Progression of DSS-Induced Colitis In Vivo with Efficacy Comparable to or Surpassing 5-ASA

In vivo, SBF dose-dependently reduced DAI scores, rescued colon length, and diminished splenomegaly, with 200 mg/kg matching or surpassing 5-ASA (Figure 3). The optimal dose is anchored to SBF's chemical richness: fermentation-enriched low-molecular-weight species [35] and the 43-compound pool likely reach a tissue-penetrating threshold at 200 mg/kg to maximally inhibit NF-κB-driven transcription. Although 5-ASA partially inhibits NF-κB [36], SBF-200 showed comparable or slightly better efficacy in this specific model, suggesting the potential benefits of multi-component products, which warrants further verification. The concurrent DAI reduction mirrors the clinical "treat-to-target" paradigm for mucosal healing [37,38], suggesting SBF may interrupts underlying immune dysregulation rather than merely alleviating symptoms.

4.4. Suppression of NF-κB Signaling and Macrophage Infiltration Underlies the Anti-Colitic Effect of SBF

SBF attenuated colonic inflammation in association with suppressed NF-κB activation and reduced macrophage infiltration. DSS challenge elevated the colonic protein levels of IL-1β, TNF-α, and IL-6; SBF dose-dependently reversed these changes, with SBF-200 comparable to or exceeding 5-ASA (Figure 4B–D). Notably, colonic IL-10 levels were elevated in the DSS group compared with the CON group, likely reflecting a compensatory host response to acute inflammation. SBF treatment reduced IL-10 levels closer to, though not fully back to, CON levels compared with the 5-ASA group (Figure 4E). This may reflect resolution of the inflammatory response, although a direct effect of SBF on IL-10-producing cells cannot be excluded; this possibility remains to be tested. Correspondingly, SBF downregulated colonic *Tnfa*, *Il6*, *Il1b*, *Ifng*, *Cox2*, and *Ccl2* mRNA expression (Figure 5B–G). Western blotting showed that SBF dose-dependently reduced DSS-induced phosphorylation of IκBα and p65 (Figure 4F–J); because NF-κB drives the transcription of *IL-1β*, *TNF-α*, *IL-6*, *COX-2*, and *MCP-1*, this coordinated decrease identifies NF-κB inhibition as a central mechanism. Representative IHC images suggested a reduction in F4/80+ macrophage infiltration (Figure 5A), IHC confirmed reduced F4/80^{+} macrophage infiltration (Figure 5A), consistent with the downregulated MCP-1 (Figure 5G).

This multi-node activity accords with the LC-MS/MS profile, in which cyclic peptides and diketopiperazines are prominent. Cyclic peptides and mushroom-derived peptides can suppress this axis at multiple nodes: the fungal cyclohexadepsipeptide beauvericin inhibits NF-κB activation and p65/p50 nuclear translocation in LPS-stimulated RAW264.7 macrophages [39]; mushroom-derived peptides downregulate IKKβ, p-IκBα and p-NF-κB in the same model [40]; and the cyclic dipeptide cyclo(His-Pro) suppresses NF-κB nuclear accumulation and the NF-κB-dependent gene COX-2 [41]. The minor constituent caffeic acid likewise ameliorates DSS colitis via NF-κB inhibition, with increased *Akkermansia* [42]—a genus also enriched by SBF here. As the identified compounds were not individually isolated or subjected to functional verification, the specific active principles of SBF remain to be determined.

4.5. SBF Remodels Gut Microbiota Composition and Promotes Microbial Homeostasis

SBF treatment altered the gut microbiota composition, notably increasing the relative abundance of *Akkermansia* and *Faecalibaculum* and reducing that of *Turicibacter*, *Clostridium*, and *Enterococcus* (Figure 6F–K). Alongside these compositional shifts, 16S rRNA sequencing showed that SBF reduced the Shannon index elevated in DSS-treated mice: SBF50 and SBF200 returned Shannon values to levels not significantly different from CON, whereas SBF100 produced a partial reduction (Figure 6A). Beta diversity based on weighted UniFrac

distances showed that CON samples clustered separately from NC, and that SBF100 and SBF200 shifted toward the CON cluster, whereas 5-ASA remained close to NC (Figure 6B). At the phylum level, SBF attenuated the DSS-induced expansion of *Proteobacteria* (represented by *Escherichia-Shigella*) and partially shifted the *Bacteroidetes*-to-*Firmicutes* ratio toward the CON profile [43,44].

Previous studies have reported that *Escherichia-Shigella* can activate the TLR4/NF-κB pathway, and that *Clostridium* and *Turicibacter* have been associated with mucosal inflammation [45]. Our data do not establish causality, but the reduction in these taxa by SBF coincided with attenuated colonic NF-κB signaling and reduced myeloid cell infiltration in our model. This raises the possibility of a bidirectional interaction, in which alleviation of mucosal inflammation and the accompanying microbial shifts reinforce each other. We present this as a hypothesis rather than a demonstrated mechanism. The concurrent modulation of inflammatory signaling and microbiota composition is consistent with the multi-component activity of SBF observed across our endpoints.

4.6. Therapeutic Implications and Future Perspectives

These findings suggest SBF as a potential fungal-derived candidate for UC, integrating NF-κB inhibition, macrophage recruitment suppression, and microbiota remodeling—a multi-node intervention that may offer advantages over single-target drugs. These findings suggest that SBF may be a candidate for further investigation in UC, combining NF-κB inhibition, reduced macrophage infiltration, and microbiota remodeling in a single preparation. Whether this multi-component profile offers advantages over single-target drugs remains to be determined. Current therapies face ~30% primary non-response to anti-TNF-α [34] and limited efficacy of 5-ASA [46,47]. The chemical diversity of SBF, coupled with its efficacy via oral administration, suggests a potential therapeutic strategy aligned with microbiome-immune cotargeting.

However, it should be noted that in this study, SBF was administered concurrently with DSS (Days 1–8), which represents a prophylactic (co-treatment) regimen rather than a therapeutic intervention for established inflammation. Therefore, the present findings support the protective potential of SBF, but the conclusions remain preliminary: with only small sample sizes ($n = 6$ for in vivo assays, $n = 3$ for 16S sequencing) statistical power was limited and the assumptions underlying parametric tests could not be fully verified. In addition, no formal a priori power calculation was performed, and dosing personnel and animal caretakers were not blinded to group allocation. Larger cohorts will be required to validate these findings. It should be noted that a concentrated uninoculated MMN medium control was not included in this study. Therefore, the possibility that medium-derived components contribute to some of the observed effects cannot be fully excluded, and our conclusions are based on dose-dependent differences between SBF-treated groups and the vehicle control rather than on absolute attribution to fungal metabolites.

Future studies should prioritize: (i) employing a therapeutic protocol to determine whether SBF can reverse pre-existing inflammation; (ii) NMR structural confirmation and fractionation-coupled bioassays; (iii) formal toxicological evaluations (e.g., acute and subchronic oral toxicity in rodents to establish the NOAEL); (iv) target deconvolution and validation in organoids and clinical trials; and (v) detailed evaluation of the effects of SBF on the Treg/Th17 balance and macrophage polarization using flow cytometry. Future work will further dissect the contribution of individual constituents by fractionation-coupled bioassays, which will also allow the activity of the complete fermentation system to be compared with that of defined sub-fractions.

5. Conclusions

In this study, we observed that SBF treatment was associated with dose-dependent alleviation of DSS-induced ulcerative colitis in mice. In LC-MS/MS profiling revealed that SBF is enriched in 43 bioactive constituents, including sclerocitrin homologs, cyclic peptides, and alkaloids, which may collectively contribute to its multi-target anti-inflammatory activity. In vitro, SBF protected RAW264.7 macrophages from LPS-induced injury, suppressed NO overproduction, and rebalanced the expression of pro-and anti-inflammatory genes. In vivo, SBF dose-dependently alleviated disease severity—reducing DAI scores, rescuing colon length, and diminishing splenomegaly—with the highest dose (200 mg/kg) exhibiting efficacy comparable to the clinical drug 5-ASA in this acute model. Mechanistically, SBF suppressed colonic inflammation by inhibiting NF-κB signaling pathway activation and reducing macrophage infiltration. Concurrently, SBF modulated the gut microbiota composition by increasing the relative abundance of *Akkermansia* and *Faecalibaculum*, while suppressing taxa such as *Clostridium*, *Escherichia-Shigella*, and *Turicibacter*. The present evidence supports a preliminary signal in one acute DSS-induced mouse model and one macrophage cell line. The specific active constituents, batch-to-batch reproducibility, detailed mechanism, and efficacy when administered after disease onset remain to be determined. The safety profile, oral bioavailability, pharmacokinetics, and human efficacy of SBF have not been established and require extensive future investigation.

Supplementary Materials: The following supporting information can be downloaded at: https://www.mdpi.com/article/10.3390/microorganisms14112673/s1, Figure S1: Six compounds detected and assigned from SBF by LC-MS/MS analysis; Table S1: Lists the primer sequences used n this study; Table S2: Using a high-resolution liquid chromatography-mass spectrometry (LC-MS) instrument, 43 substances in SBF were detected.

Author Contributions: Y.Y., investigation, writing—original draft preparation; M.Z., investigation; X.L., investigation; Y.C., investigation; S.Y., investigation; H.H., methodology; X.F., methodology; J.L., Conceptualization, writing—review and editing, funding acquisition. All authors have read and agreed to the published version of the manuscript.

Funding: This work was supported by the Natural Science Foundation of Jilin Province [Grant No. YDZJ202601ZYTS247].

Institutional Review Board Statement: This study was conducted in accordance with the ARRIVE (Animal Research: Reporting of In Vivo Experiments) guidelines. The animal protocol was approved by the Institutional Animal Care and Use Committee of Jilin Normal University. (Approval No.: KJLL20251002; Approval Date: 13 October 2025).

Informed Consent Statement: Not applicable.

Data Availability Statement: The 16S rRNA sequencing data supporting the findings of this study have been deposited in the NCBI BioProject database under accession number PRJNA1532645. Additional data related to this study are available from the corresponding author upon reasonable request.

Acknowledgments: The authors thank the Jilin Provincial Key Laboratory of Plant Resource Science and Green Production for providing the experimental platform.

Conflicts of Interest: The authors declare that this research was conducted in the absence of any commercial or financial relationships that could be construed as a potential conflict of interest.

Abbreviations

Abbreviations	Definition
Ulcerative colitis	UC
Inflammatory bowel disease	IBD
Scleroderma bovista fermentation broth	SBF
Dulbecco Minimum Essential Medium	DMEM
Dextran sulfate sodium	DSS
5-aminosalicylic acid	5-ASA
Nitric oxide	NO
Lipopolysaccharides	LPS
Calvatia lilacina	CL
Potato dextrose agar	PDA
Data-dependent acquisition	DDA
Higher-energy collisional dissociation	HCD
Cell Counting Kit-8	CCK-8
Negative Control	NC
Disease activity index	DAI
Phosphate-buffered saline	PBS
Hematoxylin-eosin	H&E
Immunohistochemical	IHC
Phosphorylated IκBα	p-IκBα
Phosphorylated p65	p-p65
Tumor necrosis factor-α	TNF-α
Interleukin-1β	IL-1β
Interleukin-6	IL-6
Interleukin-10	IL-10
Interferon-γ	IFNγ
Principal coordinate analysis	PCoA
Linear discriminant analysis effect size	LEfSe

References

1. Bruner, L.P.; White, A.M.; Proksell, S. Inflammatory bowel disease. *Prim. Care* **2023**, *50*, 411–427. [PubMed]
2. Molodecky, N.A.; Soon, I.S.; Rabi, D.M.; Ghali, W.A.; Ferris, M.; Chernoff, G.; Benchimol, E.I.; Panaccione, R.; Ghosh, S.; Barkema, H.W.; et al. Increasing incidence and prevalence of the inflammatory bowel diseases with time, based on systematic review. *Gastroenterology* **2011**, *142*, 46–54.e42. [CrossRef] [PubMed]
3. Liang, Y.; Li, Y.; Lee, C.; Yu, Z.; Chen, C.; Liang, C. Ulcerative colitis: Molecular insights and intervention therapy. *Mol. Biomed.* **2024**, *5*, 42. [CrossRef] [PubMed]
4. Adamina, M.; Kienle, P.; Chaparro, M.; Verstockt, B.; Minozzi, S.; Allocca, M.; Atreya, R.; Avellaneda, N.; Barreiro-De Acosta, M.; Battat, R.; et al. ECCO guidelines on therapeutics in ulcerative colitis: Surgical treatment. *J. Crohns Colitis* **2026**, *20*, jjag072. [CrossRef] [PubMed]
5. Wangchuk, P.; Yeshi, K.; Loukas, A. Ulcerative colitis: Clinical biomarkers, therapeutic targets, and emerging treatments. *Trends Pharmacol. Sci.* **2024**, *45*, 892–903. [CrossRef] [PubMed]
6. Cao, S.Y.; Ye, S.J.; Wang, W.W.; Wang, B.; Zhang, T.; Pu, Y.Q. Progress in active compounds effective on ulcerative colitis from Chinese medicines. *Chin. J. Nat. Med.* **2019**, *17*, 81–102. [CrossRef] [PubMed]
7. Zong, Y.; Meng, J.; Mao, T.; Han, Q.; Zhang, P.; Shi, L. Repairing the intestinal mucosal barrier of traditional Chinese medicine for ulcerative colitis: A review. *Front Pharmacol.* **2023**, *14*, 1273407. [CrossRef] [PubMed]
8. Feng, W.; Zhu, L.; Shen, H. Traditional chinese medicine alleviates ulcerativecolitis via modulating gut microbiota. *Evid. Based Complement Altern. Med.* **2022**, *2022*, 8075344. [CrossRef] [PubMed]
9. Zhang, X.; Yu, Y.; Yu, L.; Wu, C.; Chen, Y.; Wang, J.; Chen, H.; Xu, C.; Lin, J.; Zhang, X.; et al. Anti-inflammatory activity and mechanism of action of Banxia Xiexin Decoction on DSS-induced ulcerative colitis in mice. *J. Ethnopharmacol.* **2025**, *356*, 120824. [CrossRef] [PubMed]
10. Huang, Q.; Peng, W.; Luo, Q.; Zhao, W.; Dai, W.; Zeng, H.; Wong, H.L.X.; Hu, X. Exploring the mechanism of Suxin Hugan Fang in treating ulcerative colitis based on network pharmacology. *Sci. Rep.* **2024**, *14*, 27196. [CrossRef] [PubMed]
11. Zhong, Y.; Liu, W.; Xiong, Y.; Li, Y.; Wan, Q.; Zhou, W.; Zhao, H.; Xiao, Q.; Liu, D. Astragaloside IV alleviates ulcerative colitis by regulating the balance of Th17/Treg cells. *Phytomedicine* **2022**, *104*, 154287. [CrossRef] [PubMed]
12. Xia, W.; Lin, H.; Zhang, J.; Bai, Y.; Wei, Z.; Zhao, H.; Xia, Y.; Dai, Y. Hyperoside promotes autophagy of colonic epithelial cells to protect intestinal barrier function in ulcerative colitis. *Food Funct.* **2025**, *16*, 5543–5555. [CrossRef] [PubMed]

13. Cicha-Jeleń, M.; Muszynska, B.; Kala, K.; Sulkowska-Ziaja, K. Medicinal potential of the giant puffball mushroom *Calvatia gigantea* (Agaricomycetes): A review. *Int. J. Med. Mushrooms* **2024**, *26*, 13–25. [CrossRef] [PubMed]
14. Ding, X.; Yang, C.; Li, Y.; He, T.; Xu, Y.; Cheng, X.; Song, J.; Xue, N.; Min, W.; Feng, W.; et al. Reshaped commensal wound microbiome via topical application of *Calvatia gigantea* extract contributes to faster diabetic wound healing. *Burn. Trauma.* **2024**, *12*, tkae037. [CrossRef] [PubMed]
15. Yeh, C.-H.; Yang, S.-T.; Chen, C.-H. *Calvatia lilacina* protein extract induces apoptosis through endoplasmic reticulum stress in human colon carcinoma cells. *Process Biochem.* **2011**, *46*, 1599–1606. [CrossRef]
16. Zhang, S.Y.; Xu, L.T.; Li, A.X.; Wang, S.M. Effects of ergosterol, isolated from *Scleroderma polyrhizum* Pers., on lipopolysaccharide-induced inflammatory responses in acute lung injury. *Inflammation* **2015**, *38*, 1979–1985. [CrossRef] [PubMed]
17. Chassaing, B.; Aitken, J.D.; Malleshappa, M.; Vijay-Kumar, M. Dextran sulfate sodium (DSS)-induced colitis in mice. *Curr. Protoc. Immunol.* **2014**, *104*, 15.25.1–15.25.14. [CrossRef] [PubMed]
18. Xie, Q.; Li, H.; Ma, R.; Ren, M.; Li, Y.; Li, J.; Chen, H.; Chen, Z.; Gong, D.; Wang, J. Effect of *Coptis chinensis* Franch and *Magnolia officinalis* on intestinal flora and intestinal barrier in a TNBS-induced ulcerative colitis rats model. *Phytomedicine* **2022**, *97*, 153927. [CrossRef] [PubMed]
19. Khan, S.; Fiaz, M.; Alvi, I.A.; Ikram, M.; Yasmin, H.; Ahmad, J.; Ullah, A.; Niaz, Z.; Hayat, S.; Ahmad, A.; et al. Molecular profiling, characterization and antimicrobial efficacy of silver nanoparticles synthesized from *Calvatia gigantea* and *Mycena leaiana* against multidrug-resistant pathogens. *Molecules* **2023**, *29*, 5225. [CrossRef] [PubMed]
20. Bojarska, J.; Wolf, W.M. Short peptides as powerful arsenal for smart fighting cancer. *Cancers* **2024**, *16*, 3254. [CrossRef] [PubMed]
21. Shankar, S.; Tripathi, D.; Nayak, S.S.; Krishna, R.; Sakthivel, N. Prediction and assessment of anticancer, antiproliferative, pharmacokinetic properties, and human serum albumin binding propensity of a new bioactive marine cyclic dipeptide from *Exiguobacterium profundum*. *Mar. Biotechnol.* **2025**, *28*, 3. [CrossRef] [PubMed]
22. Sun, H.; Cai, W.; Wang, X.; Liu, Y.; Hou, B.; Zhu, X.; Qiu, L. *Vaccaria* hypaphorine alleviates lipopolysaccharide-induced inflammation via inactivation of NFκB and ERK pathways in Raw 264.7 cells. *BMC Complement Altern. Med.* **2017**, *17*, 120. [CrossRef] [PubMed]
23. Yao, Y.; Wang, W.; Shi, W.; Yan, R.; Zhang, J.; Wei, G.; Liu, L.; Che, Y.; An, C.; Gao, S.S. Overproduction of medicinal ergot alkaloids based on a fungal platform. *Metab. Eng.* **2021**, *69*, 198–208. [CrossRef] [PubMed]
24. Li, Q.; Zhu, J.; Lv, X.; Liu, J.; Liu, H.; Wang, Q.; Li, Y. Alterations in functional constituents and bioactivities of tartary buckwheat via solid-state fermentation with three edible-medicinal fungi: A metabolomics-based analysis. *Foods* **2025**, *14*, 4187. [CrossRef] [PubMed]
25. Long, D.; Sung, J.J. Crohn's disease and ulcerative colitis: From pathophysiology to novel therapeutic approaches. *Biomedicines* **2024**, *12*, 689. [CrossRef] [PubMed]
26. Di Rienzo, A.; Marinelli, L.; Dimmito, M.P.; Toto, E.C.; Di Stefano, A.; Cacciatore, I. Advancements in inflammatory bowel disease management: From traditional treatments to monoclonal antibodies and future drug delivery systems. *Pharmaceutics* **2024**, *16*, 1185. [CrossRef] [PubMed]
27. Escamilla-Medrano, J.A.; Londoño-Hernández, L.; Balagurusamy, N.; Hernández-Almanza, A.Y. Application of microbial pigments in the pharmaceutical industry: Current status and opportunities. *Arch. Microbiol.* **2025**, *207*, 104. [CrossRef] [PubMed]
28. Winner, M.; Giménez, A.; Schmidt, H.; Sontag, B.; Steffan, B.; Steglich, W. Unusual pulvinic acid dimers from the common fungi *Scleroderma citrinum* (common earthball) and *Chalciporus piperatus* (peppery bolete). *Angew. Chem. Int. Ed. Engl.* **2004**, *43*, 1883–1886. [CrossRef] [PubMed]
29. Ghazani, N.D.; Shojaei, A.; Rahbarnia, L.; Safary, A.; Akbarzadeh-Khiavi, M.; Nabizadeh, S. Innovations in peptide-based targeted therapies for breast cancer: From conjugates to precision delivery. *BioMed Pharmacother.* **2026**, *201*, 119707. [CrossRef] [PubMed]
30. Ji, X.; Farrera-Soler, L.; Li, J.; Sangouard, G.; De Sadeleer, N.; Nielsen, A.L.; Mothukuri, G.K.; Zarda, A.; Will, E.J.; Pojer, F.; et al. Generation of membrane-permeable cyclic peptides inhibiting protein-protein interaction. *Nat. Chem. Biol.* **2026**, *22*, 1351–1361. [CrossRef] [PubMed]
31. Ding, Y.H.; Miao, R.X.; Zhang, Q. Hypaphorine exerts anti-inflammatory effects in sepsis induced acute lung injury via modulating DUSP1/p38/JNK pathway. *Kaohsiung J. Med. Sci.* **2021**, *37*, 883–893. [CrossRef] [PubMed]
32. Kaiser, G.C.; Yan, F.; Polk, D.B. Mesalamine blocks tumor necrosis factor growth inhibition and nuclear factor kappaB activation in mouse colonocytes. *Gastroenterology* **1999**, *116*, 602–609. [CrossRef] [PubMed]
33. Zhang, Y.; Yang, D.; Jiang, J.; Wang, D.; Ji, F.; Sun, Z. The plasticity and metabolic reprogramming of macrophage in ulcerative colitis. *Front. Immunol.* **2026**, *17*, 1903462. [CrossRef] [PubMed]
34. Wang, L.F.; Chen, P.R.; He, S.K.; Duan, S.H.; Zhang, Y. Predictors and optimal management of tumor necrosis factor antagonist nonresponse in inflammatory bowel disease: A literature review. *World J. Gastroenterol.* **2023**, *29*, 4481–4498. [CrossRef] [PubMed]
35. Tešanović, K.; Pejin, B.; Šibul, F.; Matavulj, M.; Rašeta, M.; Janjušević, L.; Karaman, M. A comparative overview of antioxidative properties and phenolic profiles of different fungal origins: Fruiting bodies and submerged cultures of *Coprinus comatus* and *Coprinellus truncorum*. *J. Food Sci. Technol.* **2017**, *54*, 430–438. [CrossRef] [PubMed]

36. Bantel, H.; Berg, C.; Vieth, M.; Stolte, M.; Kruis, W.; Schulze-Osthoff, K. Mesalazine inhibits activation of transcription factor NF-kappaB in inflamed mucosa of patients with ulcerative colitis. *Am. J. Gastroenterol.* **2000**, *95*, 3452–3457. [CrossRef] [PubMed]
37. Turner, D.; Ricciuto, A.; Lewis, A.; D'Amico, F.; Dhaliwal, J.; Griffiths, A.M.; Bettenworth, D.; Sandborn, W.J.; Sands, B.E.; Reinisch, W.; et al. Stride-II: An update on the selecting therapeutic targets in inflammatory bowel disease (STRIDE) initiative of the international organization for the study of ibd (IOIBD): Determining therapeutic goals for treat-to-target strategies in IBD. *Gastroenterology* **2020**, *160*, 1570–1583. [CrossRef] [PubMed]
38. Peyrin-Biroulet, L.; Sandborn, W.; Sands, B.E.; Reinisch, W.; Bemelman, W.; Bryant, R.V.; D'Haens, G.; Dotan, I.; Dubinsky, M.; Feagan, B.; et al. Selecting therapeutic targets in inflammatory bowel disease (STRIDE): Determining therapeutic goals for treat-to-target. *Am. J. Gastroenterol.* **2015**, *110*, 1324–1338. [CrossRef] [PubMed]
39. Yoo, S.; Kim, M.Y.; Cho, J.Y. Beauvericin, a cyclic peptide, inhibits inflammatory responses in macrophages by inhibiting the NF-κB pathway. *Korean J. Physiol. Pharmacol.* **2017**, *21*, 449–456. [CrossRef] [PubMed]
40. Li, M.; Ge, Q.; Du, H.; Lin, S. *Tricholoma matsutake*-derived peptides ameliorate inflammation and mitochondrial dysfunction in RAW264.7 macrophages by modulating the NF-κB/COX-2 pathway. *Foods* **2021**, *10*, 2680. [CrossRef] [PubMed]
41. Minelli, A.; Grottelli, S.; Mierla, A.; Pinnen, F.; Cacciatore, I.; Bellezza, I. Cyclo (His-Pro) exerts anti-inflammatory effects by modulating NF-κB and Nrf2 signalling. *Int. J. Biochem Cell Biol.* **2011**, *44*, 525–535. [CrossRef] [PubMed]
42. Zhang, Z.; Wu, X.; Cao, S.; Wang, L.; Wang, D.; Yang, H.; Feng, Y.; Wang, S.; Li, L. Caffeic acid ameliorates colitis in association with increased *Akkermansia* population in the gut microbiota of mice. *Oncotarget* **2016**, *7*, 31790–31799. [CrossRef] [PubMed]
43. Walujkar, S.A.; Dhotre, D.P.; Marathe, N.P.; Lawate, P.S.; Bharadwaj, R.S.; Shouche, Y.S. Characterization of bacterial community shift in human Ulcerative Colitis patients revealed by Illumina based 16S rRNA gene amplicon sequencing. *Gut Pathog.* **2014**, *6*, 22. [CrossRef] [PubMed]
44. Shah, D.; Phan, F.; Yu, Z.; Choi, J.D.W.; Toh, J.W.T. Is the microbiome the answer to inflammatory bowel disease: Systematic review. *Langenbecks Arch. Surg.* **2025**, *411*, 2. [CrossRef] [PubMed]
45. Wang, H.G.; Zhang, M.N.; Wen, X.; He, L.; Zhang, M.H.; Zhang, J.L.; Yang, X.Z. Cepharanthine ameliorates dextran sulphate sodium-induced colitis through modulating gut microbiota. *Microb. Biotechnol.* **2022**, *15*, 2208–2222. [CrossRef] [PubMed]
46. Sutherland, L.; Macdonald, J.K. Oral 5-aminosalicylic acid for maintenance of remission in ulcerative colitis. *Cochrane Database Syst. Rev.* **2006**, *10*, CD000544. [CrossRef] [PubMed]
47. Barberio, B.; Segal, J.P.; Quraishi, M.N.; Black, C.J.; Savarino, E.V.; Ford, A.C. Efficacy of oral, topical, or combined oral and topical 5-aminosalicylates, in ulcerative colitis: Systematic review and network meta-analysis. *J. Crohns Colitis* **2021**, *15*, 1184–1196. [CrossRef] [PubMed]

Disclaimer/Publisher's Note: The statements, opinions and data contained in all publications are solely those of the individual author(s) and contributor(s) and not of MDPI and/or the editor(s). MDPI and/or the editor(s) disclaim responsibility for any injury to people or property resulting from any ideas, methods, instructions or products referred to in the content.